Journal of Metals, Materials and Minerals, 35(3), e2322, 2025

The effect of Pt and Pd decoration on SnO_2 slant nanorods fabricated using DC magnetron sputtering with OAD technique for CO gas sensing applications

Nampueng PANGPAIBOON[1,*], Thitiporn KAEWYOU[1], Sethavut DUANGCHAN[1], Kata JARUWONGRUNGSEE[2], Manatsawee SRIRAK[2], Tossaporn LERTVANITHPHOL[2], Viyapol PATTHANASETTAKUL[2], Tawee POGFAY[2], Mati HORPRATHUM[2], and Saksorn LIMWICHEAN[2,*]

[1] *Department of Industrial Physics and Medical Instrumentation, Faculty of Applied Science, King Mongkut's University of Technology North Bangkok, Bangkok, 10800, Thailand*

[2] *National Electronics and Computer Technology Center (NECTEC), National Science and Technology Development Agency, Pathum Thani, 12120 Thailand*

***Corresponding author e-mail**: Nampueng.p@sci.kmutnb.ac.th, Saksorn.limwichean@nectec.or.th

Received date:
27 December 2024
Revised date:
24 February 2025
Accepted date:
4 May 2025

Keywords:
SnO_2 slant nanorods;
Pt nanoparticles;
Pd nanoparticles;
Oblique angle deposition;
Magnetron sputtering

Abstract

This research investigates the effect of Pt and Pd decoration on the structure of SnO_2 slant nanorods (SNRs) films produced using DC magnetron sputtering with Oblique Angle Deposition (OAD), as well as their impact on the films' physical properties and gas sensing applications. Pt and Pd were deposited onto the SnO_2 SNRs for the same duration of 20 s each. Following deposition, all the films were heat-treated temperature at 400°C for 2 h. The characterization of both as-deposited and annealed films involved analyzing the physical morphology using FE-SEM and the crystal structure using GI-XRD. It was observed that the structure of the SnO_2 SNRs showed no significant differences before and after decoration. XRD analysis identified the crystalline structure of SnO_2 at the (110), (101), and (211) planes. After decoration, additional peaks corresponding to Pt at (111) and (200) and Pd at (111) were detected. Additionally, TEM mapping revealed that most of the deposited particles were largely concentrated on the top surface of the nanorods. Finally, testing for CO gas sensing performance revealed that the SnO_2 SNRs decorated with Pt demonstrated the highest sensitivity, detecting CO gas at concentrations as low as 50 ppm.

1. Introduction

Global warming has become a pressing issue in recent years, mainly due to the release of pollutants into the atmosphere, such as ozone (O_3), nitrogen dioxide (NO_x, NO_2), sulfur dioxide (SO_2), volatile organic compounds (VOCs), and carbon monoxide/dioxide (CO, CO_2) [1,2]. Consequently, the demand for energy-efficient and highly sensitive gas sensors has grown to help monitor and manage emissions in various settings. This is particularly important for indoor environments, including homes, schools, and offices, where pollutant levels can be 2 time to 5 time higher than those outdoors, and individuals spend nearly 90% of their time [3]. The current gas sensor market provides a diverse range of metal oxide semiconductor (MOS) based gas sensors for monitoring various gases. These sensors are highly favored due to their low cost, ease of fabrication, high electron mobility, excellent conductivity, and robust physical, mechanical, and chemical stability [4,5]. Several methods have been developed to improve the performance of MOS gas sensors, such as noble metal modification [6], doping [7], and nanostructuring [8]. These techniques play a crucial role in optimizing sensor performance for various applications [9,10].

Nanostructures of widely studied MOS gas-sensing materials, such as WO_3 [11,12], ZnO [13,14], TiO_2 [15,16], and SnO_2 [17,18], have demonstrated enhanced sensitivity and faster response times at low gas concentrations compared to conventional thin films. Among these, SnO_2 nanostructure films, a wide bandgap n-type semiconductor, are highly popular due to their excellent conductivity, rapid response, low operating temperature, and high stability [19-22]. A prominent method for fabricating SnO_2 nanostructures is reactive magnetron sputtering combined with oblique angle deposition (OAD) and glancing-angle deposition (GLAD). This technique involves tilting the substrate holder at an angle greater than 80° relative to the coating material flux from the sputtering cathode and precisely controlling substrate rotation. Such an approach enables the production of nanostructured thin films with adjustable porosity and shapes by utilizing the self-shadowing effect and surface diffusion during deposition [23,24]. This method facilitates the creation of various nanostructures, including nanorods, slant nanorods, zigzag, and spiral configurations [25,26]. It is a cost-effective, single-step process that eliminates chemical residues, provides precise control over deposition conditions, supports direct growth on substrates, and is easily scalable for mass production [17,27].

Despite advancements in MOS nanostructures for gas sensing, their sensitivity may still be inadequate for detecting gases at low concentrations. To address this limitation, noble metals such as Pt, Pd, Ag, and Au are often integrated into the sensors to enhance catalytic efficiency [7,28,29]. This improvement is attributed to their synergistic and catalytic effects, as noble metals promote both electronic and

chemical sensitization. Specifically, they lower the activation energy by expanding the electron depletion layer and catalyzing gas reactions [30-32]. Previous studies have compared noble metal nanoparticles for enhancing the sensitivity of SnO_2 octahedra-based VOC gas sensors [33] However, the preparation of such structures involves chemical synthesis processes, which generate chemical waste and pose challenges for large-scale production. Moreover, these studies did not include testing for CO gas, a critical atmospheric pollutant produced by incomplete combustion.

This study focuses on comparing the effects of Pt and Pd decoration on SnO_2 slant nanorods (SNRs) films, fabricated via reactive DC magnetron sputtering using the oblique angle deposition (OAD) technique. The sputtering duration for decoration was kept identical for both materials. After film preparation, studies were conducted on the physical properties, crystallinity, and the adhesion and distribution of the elemental/compound composition. Furthermore, the films were prepared on interdigitated electrodes fabricated on a low-temperature co-fired ceramic (LTCC) substrate to evaluate their performance in detecting CO gas in a concentration range of 50 ppm to 1000 ppm.

2. Experimental

The SnO_2 SNRs films were fabricated using DC magnetron sputtering with oblique angle deposition (OAD) onto silicon (Si) and electrode substrates. A 3 inch tin (Sn) metal target with a purity of 99.99% (provided by Kurt J. Lesker Company) was utilized for the deposition process. Before deposition, the substrates were thoroughly cleaned with deionized water and ethanol to ensure surface cleanliness before being placed inside the sputtering chamber. The sputtering process was conducted under a gas mixture of argon (Ar, 99.999%) and oxygen (O_2, 99.999%) with flow rates of 20 sccm and 60 sccm, respectively. The base pressure was maintained at 5×10^{-6} mbar, and the working pressure was set to 3.0×10^{-3} mbar. The substrate was tilted at an angle of 85° degrees relative to the vapor flux, as illustrated in the schematic diagram in Figure 1. During the deposition process, DC power was set to 150 W for 30 min. After deposition, the as-deposited SnO_2 SNRs films were subjected to decorate noble metal (Pd and Pt) in magnetron sputtering by DC power set to 100 W for 20 s. The decorated films were then annealed in ambient air at 400°C for 2 h under all conditions.

The physical morphology of all prepared SnO_2 SNRs films was characterized using a field-emission scanning electron microscope (FE-SEM; Hitachi High Tech. SU8030). Their crystal structure was analyzed via grazing incidence X-ray diffraction (GIXRD, Rigaku). Detailed morphology and elemental/compound composition analyses were conducted on a single SnO_2 SNRs sample in its annealed state. For this, the nanorods were scraped onto a copper grid and examined using a transmission electron microscope (TEM; JEOL, JEM-2100 Plus). Energy dispersive spectroscopy (EDS) was also used to map the elements Sn, O, Pd, and Pt. High-resolution transmission electron microscopy (HR-TEM) images and selective area electron diffraction (SAED) patterns were also specifically analyzed at the tips of the nanorods.

For CO gas detection, the gas sensor in this study employed interdigitated electrodes fabricated on a micro-bridge-type micro-hotplate integrated onto a low-temperature co-fired ceramic (LTCC) substrate. This micro-hotplate was developed by the National Electronics and Computer Technology Center (NECTEC) as part of the "GAS Sensing with Easy-effective Technology (GASSET)" project. The LTCC-based version, referred to as LTCC-GASSET, is detailed in Thai Patent No. 2301005878, titled "Gas sensing device, its fabrication, and signal analysis process thereof. The main structure of the LTCC bridge featured a width of 130 μm and a length of 800 μm, with a thickness of approximately 46 μm. Platinum interdigitated electrodes (200 μm long) were coated on the top surface of the bridge, while the bottom surface was equipped with a micro-heater. According to the manufacturer's specifications, the bridge is capable of achieving a working temperature exceeding 400°C while consuming approximately 70 mW of heating power. When the SnO_2 SNRs films are coated onto the electrodes, they are subjected to heat treatment at the same temperature mentioned during the sample preparation process. For the electrical connection to the gas sensor chip, the LTCC gas sensor chip is directly soldered onto a PCB base using a standard soldering iron. Notably, the direct soldering capability between the LTCC chip and the PCB is a key feature of the LTCC-GASSET gas sensor. This eliminates the need for the high-cost wire-bonding process typically required in microelectronic devices.

3. Results and discussion

The experimental results of this study begin with the physical characterization of SnO_2 SNRs, both in their as-deposited state and after decoration with Pd and Pt, using a Field Emission Scanning Electron Microscope (FE-SEM). As shown in Figure 1(a-f), the surface and cross-sectional images indicate that the surface features remain nearly identical before and after decoration, exhibiting no significant differences. The cross-sectional analysis highlights the SNRs structure of the film, with a thickness of 727 nm and a nanorod length of 978 nm, neither of which are impacted by the decoration process. Following post-annealing at 400°C, the film maintains its overall appearance, but the thickness and nanorod length decrease to 689 nm and 944 nm, respectively. This reduction is characteristic of films undergoing thermal treatment, where atomic diffusion promotes structural reorganization, leading to reduced porosity and increased density [34].

The crystallinity of all samples was examined using a GI-XRD instrument. The XRD pattern analysis reveals that the as-deposited SnO_2 SNRs, as shown in Figure 2(a), exhibit crystallinity in the (110), (101), (200), (211), and (220) planes. This is consistent with the tetragonal rutile phase (JCPDS #01-075-2893) [35]. The Pd-decorated film exhibited a peak corresponding to the (111) plane of Pd at 39.94° (JCPDS #01-087-0643) [36]. Additionally, the Pt-decorated film displayed peaks at the (111) and (200) planes of Pt, located at 39.88° and 46.28°, respectively (JCPDS #01-085-5676) [37]. The crystallinity of the SnO_2 SNRs films and Pt-decorated films slightly improved upon post-annealing. This improvement is due to the movement and rearrangement of atoms in the material, which facilitates the formation of larger and more ordered crystals [38]. However, in the Pd-decorated film, the (111) plane disappeared, while peaks corresponding to the (101) and (110) planes emerged at 34.24° and 42.02°, respectively, indicating the formation of PdO (JCPDS #04-005-4230) [39]. This result confirms that Pd oxidizes with oxygen in the ambient after post-annealing. This observation aligns with previous studies, which report that Pd readily transforms into the PdO phase when subjected to post-annealing in atmospheric [40,41].

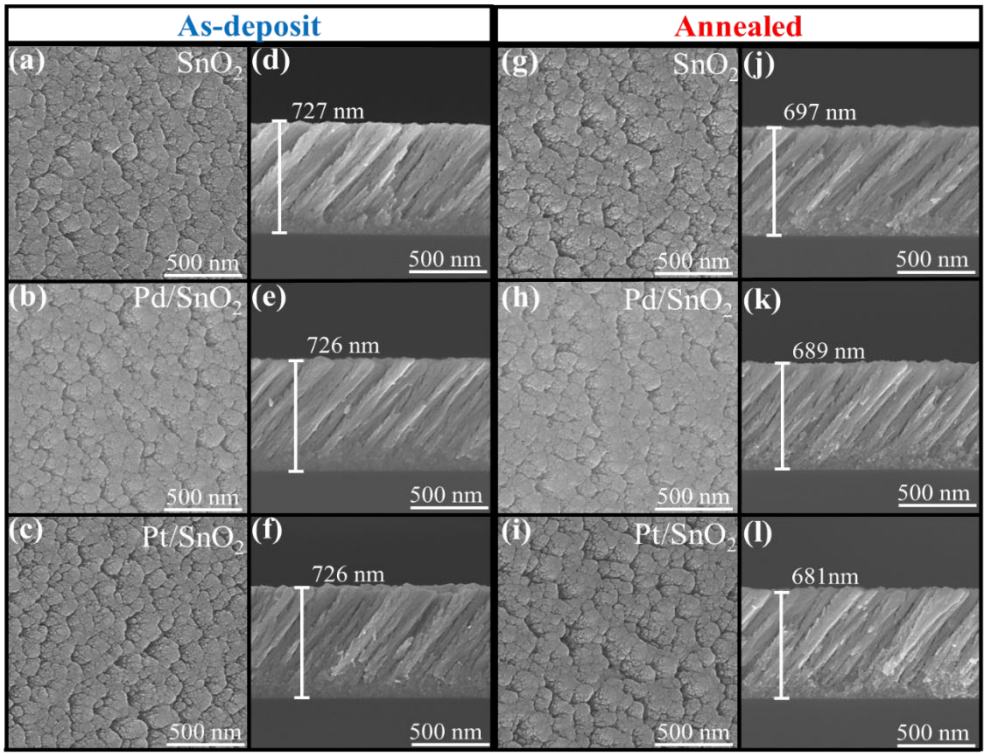

Figure 1. Top-view and cross-sectional FE-SEM images of the SnO_2 SNRs are presented for (a-f) the as-deposited (ASD) samples and (g-l) the annealed samples treated at 400°C for 2 hours. The images correspond to different decoration conditions: pure SnO_2, Pd-decorated, and Pt-decorated samples.

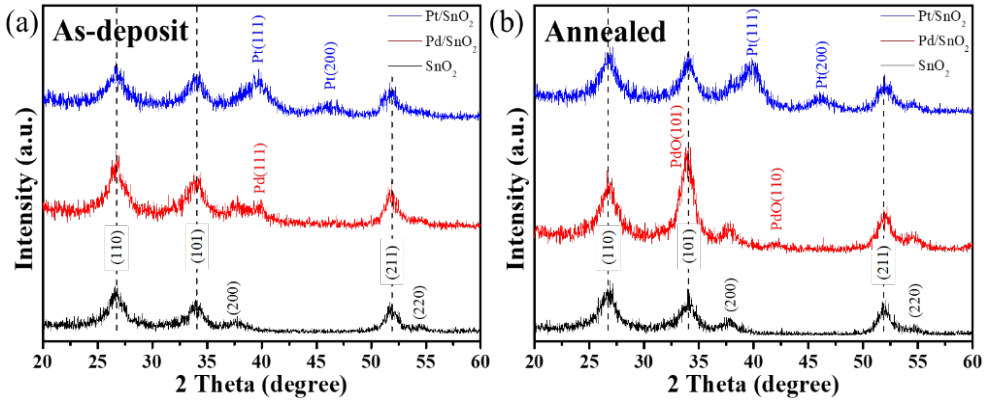

Figure 2. GI-XRD spectra of (a) as-deposited (ASD) and (b) annealed SnO_2 SNRs with different decorations: pure SnO_2, Pd-decorated, and Pt-decorated samples.

The typical EDS spectra of all films are presented in Figure 3(a-b), clearly indicating the dispersive energy peaks of Sn and O. Additionally, C peaks are observed, which are attributed to partial contamination and surface formation on the films. Furthermore, the spectra of the decorated SnO_2 SNRs films distinctly show the presence of Pd and Pt. The Si peak, originating from the silicon substrate, was observed in all thin films. After heat treatment, a slight increase in the O composition was detected, suggesting improved film properties [42]. In addition, Pd and Pt remain integrated within the SnO_2 SNRs films, with their atomic compositions remaining nearly constant. This is evident from the percentage of atomic composition for Sn, O, Pd, and Pt, as presented in the inserted table within the EDS spectra graph.

This observation aligns well with the XRD pattern results and HR-TEM analysis, including the selected area electron diffraction (SAED) patterns, as shown in Figure 4. The SnO_2 phase exhibited inter-planar d-spacing values of 0.335 nm and 0.264 nm, with the SAED patterns clearly reflecting the main peaks of SnO_2, corresponding to the (110) and (101) planes. Additionally, for samples decorated with Pd, an inter-planar d-spacing of 0.263 nm, attributed to PdO, was observed along with the SAED pattern in the (101) plane, confirming the XRD results. Similarly, for SnO_2 SNRs films decorated with Pt, the SAED pattern displayed diffraction at the (111) plane of Pt, with an inter-planar d-spacing of 0.226 nm. Moreover, the elemental distribution of SnO_2 SNRs films under all post-annealing conditions was analyzed using TEM-EDS mapping, as illustrated in Figure 5. The slant nanorod mapping images of all samples reveal a uniform distribution of Sn and O. Interestingly, the SnO_2 SNRs films decorated with Pd and Pt for 20 s exhibit a consistent pattern, with the decorations primarily located at the top of the nanorods, highlighted in the blue regions of the mapping images.

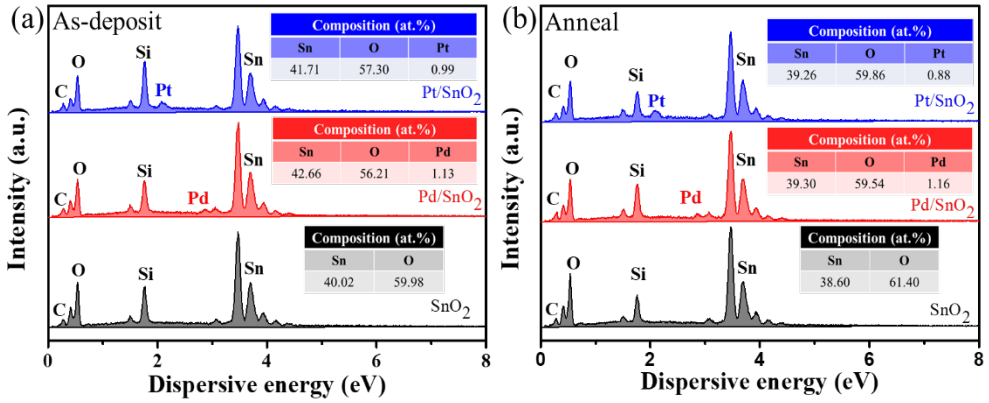

Figure 3. EDS spectra of (a) as-deposited (ASD) and (b) annealed SnO_2 SNRs with different decorations: pure SnO_2, Pd-decorated, and Pt-decorated samples.

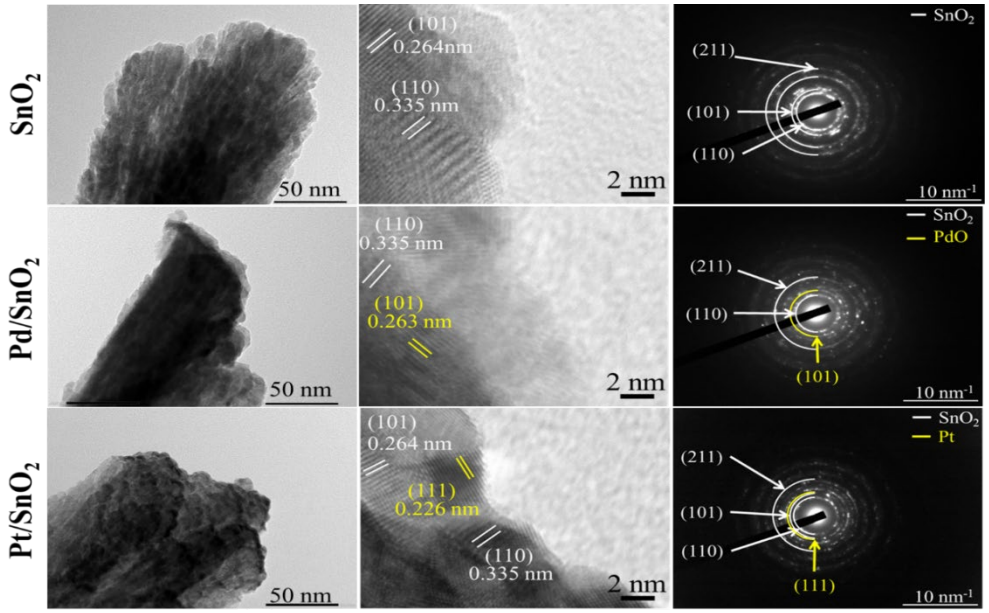

Figure 4. Associated HR-TEM images and SAED patterns of annealed SnO_2 SNRs with different decorations: pure SnO_2, Pd-decorated, and Pt-decorated samples.

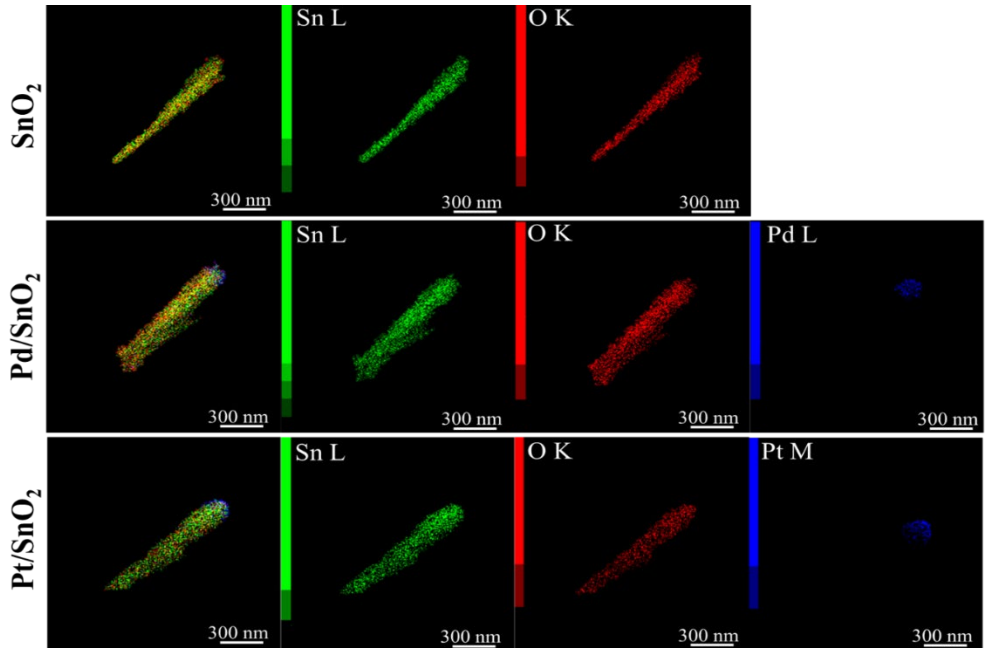

Figure 5. TEM-EDS mapping images of annealed SnO_2 SNRs with different decorations: pure SnO_2, Pd-decorated, and Pt-decorated samples.

The performance of the fabricated sensor for CO gas detection was tested under a controlled atmosphere in a chamber constructed using 3D printing as shown in Figure 6(a). The gas flow consisted of a mixture of CO and air zero (dry air) within the system, with the total flow rate maintained at 200 sccm. The flow rates were precisely controlled using a computer-controlled multi-channel mass flow controller. The resistance of the electrode was measured under a heating voltage (HV) ranging from 2.7 V to 3.2 V, corresponding to a power consumption of 37 mW to 50 mW, with CO concentrations varying between 50 ppm to 1000 ppm. The sensor response (S) for CO gas was defined according to the standard convention for reducing gases as: $S = R_{air}/R_{gas}$ where R_{air} and R_{gas} represent the stable electrical resistance of the sensor in air and in the presence of the target gas, respectively. It was observed that the SnO_2 SNRs films exhibited a lower response compared to the films decorated with Pd and Pt across all heating voltage ranges, as shown in Figure 6(b). This highlights the catalytic effect of Pd and Pt attached to the surface of the nanorods, which enhances gas response. The catalytic properties of noble metals facilitate the dissociation of O_2 molecules and increase oxygen adsorption on the SnO_2 surface, resulting in improved sensitivity and faster response to CO gas [43,44]. However, in this study, it was observed that the gas response increased with an increase in operating temperature, which contrasts with findings from previous research [43,45]. The relatively large thickness of the nanorod structure causes a delay in achieving uniform heating throughout the entire rod. Furthermore, noble metal particles are only located at the tips of the nanorods. As a result, a relatively high operating temperature is still required to increase the density of chemisorbed oxygen species (O^- and O_2^-) [17,46]. The maximum response was observed at a heating voltage of 3.1 V (equivalent to 48 mW), corresponding to an operating temperature of approximately 270°C.

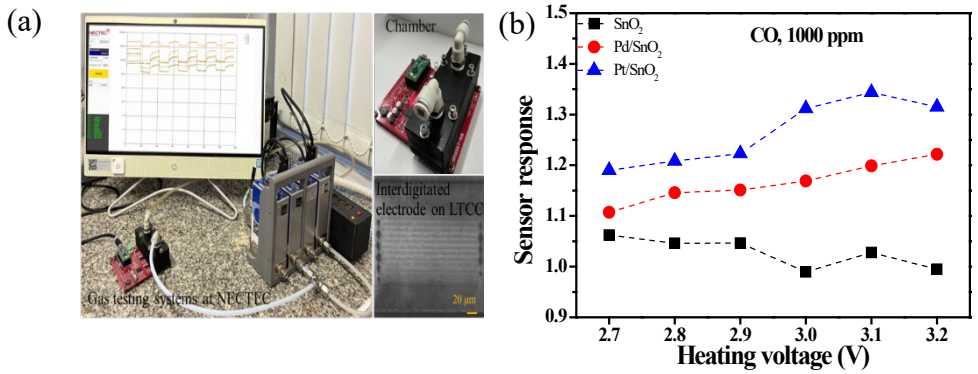

Figure 6. (a) Gas sensing test system with interdigitated electrode and (b) sensor response to 1000 ppm CO for the heating voltage of the annealed SnO_2 SNRs with different decorations: pure SnO_2, Pd-decorated, and Pt-decorated samples.

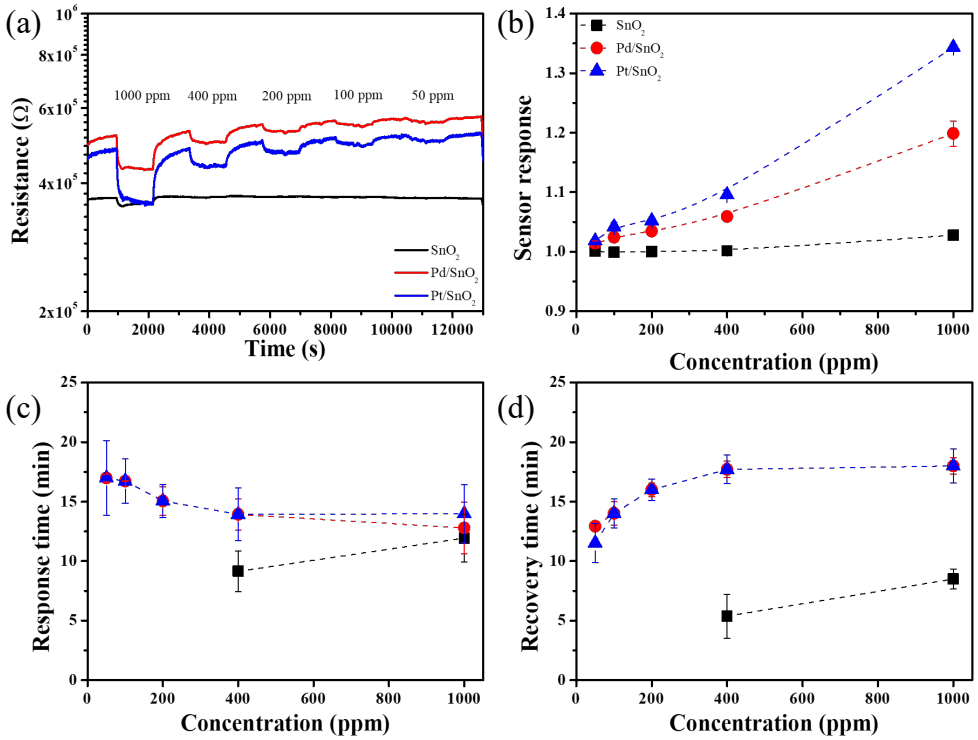

Figure 7. (a) Dynamic response of the gas sensor, (b) sensor response, (c) response time, and (d) recovery time as a function of the CO concentration at the optimal heating voltage of 3.1V.

Table 1. Summary of CO gas sensing performance based on SnO_2 prepared by various synthesis methods.

S.No.	Materials	Systhesis methods	Operate temp. [°C]	Conc. [ppm]	Resp. Ra/Rg	Ref.
1	Ca-SnO_2 nanocrystals	Magnetron sputtering	350	30	1.50	[50]
2	Pd-SnO_2 nanowires	Thermal evaporation	400	200	6.80	[51]
6	Pd-SnO_2 nannoflakes	Microwave assisted	100	200	7.00	[43]
7	Pd-SnO_2 nanorods	PECVD	250	1000	24.00	[52]
8	Pd-SnO_2 nanoparticles	Flame-spray	200	50	1.50	[53]
9	Pd-SnO_2 nanofibers	Electrospinning	160	100	1.10	[54]
11	Pt-SnO_2 nanoneedles	Hydrothermal	250	100	23.18	[55]
10	Pt-SnO_2 slant nanorods	Magnetron sputtering	270	50	1.02	This work

Figure 7(a) illustrates the current response signal of the sensor to varying concentrations of CO gas, demonstrating that SnO_2 SNRs decorated with Pd and Pt effectively respond to CO concentrations ranging from 50 ppm to 1000 ppm. It is noteworthy that the initial resistance of Pd/SnO_2 SNRs is higher than that of Pt/SnO_2 SNRs films, indicating the behavior of Pd transitioning into PdO phase [47]. When considering the response to CO gas at all concentrations, it is evident that Pt-decorated SnO_2 SNRs exhibit better gas response compared to Pd-decorated SnO_2 SNRs, as shown in Figure 7(b). The mechanism of CO and O_2 adsorption on the Pt/SnO_2 catalyst can be explained by the Langmuir-Hinshelwood (LH) model, consistent with findings reported in the literature [48]. In contrast, the XRD results confirmed that Pd in Pd/SnO_2 was oxidized to PdO, which acts as a catalyst to enhance the reaction. Consequently, the gas response of Pd/SnO_2 remains higher than that of pure SnO_2 SNRs films without noble metal decoration [47,49]. Additionally, the response and recovery times improved across various gas concentrations with the decoration of noble metals on SnO_2 SNRs films, as illustrated in Figure 7(c-d). At a CO concentration of 1000 ppm, the films demonstrated a moderate response time of approximately 13.5 min and a recovery time of 18 min. The gas detection results highlight the catalytic effect of noble metals in enhancing gas detection performance. This study demonstrates that Pt/SnO_2 SNRs films exhibit the highest efficiency in detecting CO gas.

Table 1 shows that the gas response observed in this study is lower than values reported in the literature, which may be attributed to the limited distribution of noble metal nanoparticles, primarily located on the top surfaces of the nanorods. This non-uniform coverage may lead to incomplete coverage of active sites and limit the effectiveness of the spillover effect, thereby reducing CO detection efficiency. It also likely hinders the formation of effective Schottky junctions. To address this, future work could focus on tailoring nanorod morphology, such as increasing inter-rod spacing, and optimizing the deposition conditions of noble metal sputtering, such as deposition time, operating pressure, and sputtering power, to improve the uniformity and density of nanoparticle distribution, especially along the sidewalls. These improvements would promote better electron transfer, extend the depletion region, and ultimately enhance gas-sensing performance [11].

4. Conclusions

This research successfully prepared SnO_2 SNRs decorated with Pd and Pt using DC reactive magnetron sputtering combined with the OAD technique. FE-SEM and TEM mapping results clearly showed that the noble metal particles, Pd and Pt, were uniformly distributed on the top regions of the nanorods. This uniform distribution makes them well-suited for a comparative evaluation of their gas detection performance. XRD analysis revealed a slight increase in crystallinity of the films after annealing at 400°C, demonstrating the high quality of SnO_2 SNRs films produced by the magnetron sputtering technique. Furthermore, the phase transformation of Pd to PdO due to oxidation was observed and confirmed by SAED patterns. Gas-sensing measurements showed that Pt/SnO_2 SNRs exhibited a higher response to CO gas than Pd/SnO_2 SNRs and undoped SnO_2 SNRs films, with the capability to detect gas concentrations as low as 50 ppm. While the gas response values reported in this study are relatively low compared to other research, optimization of Pt deposition sputtering time or improved interdigitated electrode designs could enhance performance. Despite this, the study successfully demonstrated a comparative evaluation of CO gas detection performance, underscoring the superior effectiveness of Pt for gas sensing. These findings provide valuable insights for advancing the development of CO gas detection devices.

Acknowledgements

This work was supported by National Electronics and Computer Technology Center (NECTEC), Thailand. The authors are likewise grateful to Opto-Electrochemical Sensing Research Team, Spectroscopic and Sensing Devices Research Group, Synchrotron Light Research Institute (SLRI). The authors would like to acknowledge research funded by King Mongkut's University of Technology North Bangkok, Contract no. KMUTNB-67-BASIC-04.

References

[1] D. Fowler, P. Brimblecombe, J. Burrows, M. R. Heal, P. Grennfelt, D. S. Stevenson, A. Jowett, E. Nemitz, M. Coyle, X. Liu, Y. Chang, G. W. Fuller, M. A. Sutton, Z. Klimont, M. H. Unsworth, and M. Vieno, "A chronology of global air quality," *Philosophical Transactions of the Royal Society A: Mathematical, Physical and Engineering Sciences*, vol. 378, no. 2183, p. 20190314, 2020.

[2] X. Ma, T. Zhang, C. Ji, Y. Zhai, X. Shen, and J. Hong, "Threats to human health and ecosystem: Looking for air-pollution related damage since 1990," *Renewable and Sustainable Energy Reviews*, vol. 145, p. 111146, 2021.

[3] P. Kumar, A. B. Singh, T. Arora, S. Singh, and R. Singh, "Critical review on emerging health effects associated with the indoor air quality and its sustainable management," *Science of The Total Environment*, vol. 872, p. 162163, 2023.

[4] D. Y. Nadargi, A. Umar, J. D. Nadargi, S. A. Lokare, S. Akbar, I. S. Mulla, S. S. Suryavanshi, N. L. Bhandari, and M. G. Chaskar, "Gas sensors and factors influencing sensing mechanism with a special focus on MOS sensors," *Journal of Materials Science*, vol. 58, no. 2, pp. 559-582, 2023.

[5] X. Gao, and T. Zhang, "An overview: Facet-dependent metal oxide semiconductor gas sensors," *Sensors and Actuators B: Chemical*, vol. 277, pp. 604-633, 2018.

[6] H. R. Yousefi, B. Hashemi, A. Mirzaei, H. Roshan, and M. H. Sheikhi, "Effect of Ag on the ZnO nanoparticles properties as an ethanol vapor sensor," *Materials Science in Semiconductor Processing*, vol. 117, p. 105172, 2020.

[7] M. Hübner, N. Bârsan, and U. Weimar, "Influences of Al, Pd and Pt additives on the conduction mechanism as well as the surface and bulk properties of SnO_2 based polycrystalline thick film gas sensors," *Sensors and Actuators B: Chemical*, vol. 171-172, pp. 172-180, 2012.

[8] S. Acharyya, and P. Kumar Guha, "Enhanced formaldehyde sensing performance employing plasma-treated hierarchical SnO_2 nanosheets through oxygen vacancy modulation," *Applied Surface Science*, vol. 655, p. 159640, 2024.

[9] R. Alrammouz, J. Podlecki, P. Abboud, B. Sorli, and R. Habchi, "A review on flexible gas sensors: From materials to devices," *Sensors and Actuators A: Physical*, vol. 284, pp. 209-231, 2018.

[10] J.-H. Kim, A. Mirzaei, H. W. Kim, and S. S. Kim, "Low-voltage-driven sensors based on ZnO nanowires for room-temperature detection of NO_2 and CO gases," *ACS Applied Materials & Interfaces*, vol. 11, no. 27, pp. 24172-24183, 2019.

[11] M. Horprathum, T. Srichaiyaperk, B. Samransuksamer, A. Wisitsoraat, P. Eiamchai, S. Limwichean, C. Chananonnawathorn, K. Aiempanakit, N. Nuntawong, V. Patthanasettakul, C. Oros, S. Porntheeraphat, P. Songsiriritthigul, H. Nakajima, A. Tuantranont, and P. Chindaudom, "Ultrasensitive hydrogen sensor based on Pt-decorated WO_3 nanorods prepared by glancing-angle DC magnetron sputtering," *ACS Applied Materials & Interfaces*, vol. 6, no. 24, pp. 22051-22060, 2014.

[12] X. Li, L. Fu, H. Karimi-Maleh, F. Chen, and S. Zhao, "Innovations in WO_3 gas sensors: Nanostructure engineering, functionalization, and future perspectives," *Heliyon*, vol. 10, no. 6, p. e27740, 2024.

[13] E. Wongrat, N. Chanlek, C. Chueaiarrom, W. Thupthimchun, B. Samransuksamer, and S. Choopun, "Acetone gas sensors based on ZnO nanostructures decorated with Pt and Nb," *Ceramics International*, vol. 43, pp. S557-S566, 2017.

[14] M. Bonyani, S. M. Zebarjad, A. Mirzaei, T.-U. Kim, H. W. Kim, and S. S. Kim, "Electrospun ZnO hollow nanofibers gas sensors: An overview," *Journal of Alloys and Compounds*, vol. 1001, p. 175201, 2024.

[15] S. Suriyawong, J. Khumphon, R. Rattanakam, P. Chaopanich, S. Thongmee, S. Youngjan, P. Khemthong, and S. Kityakarn, "Engineering three-dimensionally ordered mesoporous structure of TiO_2 for the fast responsive NH_3 gas sensor at ambient conditions," *Colloids and Surfaces A: Physicochemical and Engineering Aspects*, vol. 666, p. 131281, 2023.

[16] G. J. Thangamani and S. K. K. Pasha, "Titanium dioxide (TiO_2) nanoparticles reinforced polyvinyl formal (PVF) nanocomposites as chemiresistive gas sensor for sulfur dioxide (SO_2) monitoring," *Chemosphere*, vol. 275, p. 129960, 2021.

[17] C. Oros, M. Horprathum, A. Wisitsoraat, T. Srichaiyaperk, B. Samransuksamer, S. Limwichean, P. Eiamchai, D. Phokharatkul, N. Nuntawong, C. Chananonnawathorn, V. Patthanasettakul, A. Klamchuen, J. Kaewkhao, A. Tuantranont, and P. Chindaudom, "Ultra-sensitive NO_2 sensor based on vertically aligned SnO_2 nanorods deposited by DC reactive magnetron sputtering with glancing angle deposition technique," *Sensors and Actuators B: Chemical*, vol. 223, pp. 936-945, 2016.

[18] X. Tian, Z. Hu, C. Jia, H. Wang, and X. Wei, "A review of advanced gas sensor based on sputtering SnO_2 thin film—Challenges and opportunities," *Journal of Environmental Chemical Engineering*, vol. 11, no. 6, p. 111516, 2023.

[19] Z. Li, W. Zeng, and Q. Li, "SnO_2 as a gas sensor in detection of volatile organic compounds: A review," *Sensors and Actuators A: Physical*, vol. 346, p. 113845, 2022.

[20] Y. Kong, Y. Li, X. Cui, L. Su, D. Ma, T. Lai, L. Yao, X. Xiao, and Y. Wang, "SnO_2 nanostructured materials used as gas sensors for the detection of hazardous and flammable gases: A review," *Nano Materials Science*, vol. 4, no. 4, pp. 339-350, 2022.

[21] G. Domènech-Gil, J. Samà, C. Fàbrega, I. Gràcia, C. Cané, S. Barth, and A. Romano-Rodríguez, "Highly sensitive SnO_2 nanowire network gas sensors," *Sensors and Actuators B: Chemical*, vol. 383, p. 133545, 2023.

[22] X. Kang, N. Deng, Z. Yan, Y. Pan, W. Sun, and Y. Zhang, "Resistive-type VOCs and pollution gases sensor based on SnO_2: A review," *Materials Science in Semiconductor Processing*, vol. 138, p. 106246, 2022.

[23] H. Zhu, W. Cao, G. K. Larsen, R. Toole, and Y. Zhao, "Tilting angle of nanocolumnar films fabricated by oblique angle deposition," *Journal of Vacuum Science & Technology B, Nanotechnology and Microelectronics: Materials, Processing, Measurement, and Phenomena*, vol. 30, no. 3, 2012.

[24] B. Angel, B. Ana, R. G.-E. Agustin, and P. Alberto, "Perspectives on oblique angle deposition of thin films: From fundamentals to devices," *Materials Chemistry and Physics*, vol. 76, pp. 59-153, 2016.

[25] C. Patzig, A. Miessler, T. Karabacak, and B. Rauschenbach, "Arbitrarily shaped Si nanostructures by glancing angle ion beam sputter deposition," *Physica Status Solidi (b)*, vol. 247, no. 6, pp. 1310-1321, 2010.

[26] J. Dervaux, P.-A. Cormier, P. Moskovkin, O. Douheret, S. Konstantinidis, R. Lazzaroni, S. Lucas, and R. Snyders, "Synthesis of nanostructured Ti thin films by combining glancing angle deposition and magnetron sputtering: A joint experimental and modeling study," *Thin Solid Films*, vol. 636, pp. 644-657, 2017.

[27] S. Limwichean, N. Kasayapanand, C. Ponchio, H. Nakajima, V. Patthanasettakul, P. Eiamchai, G. Meng, and M. Horprathum, "Morphology-controlled fabrication of nanostructured WO_3 thin films by magnetron sputtering with glancing angle deposition for enhanced efficiency photo-electrochemical water splitting," *Ceramics International*, vol. 47, no. 24, pp. 34455-34462, 2021.

[28] X. Li, H. Zhang, C. Chen, H. Zhang, C. Yang, and X. Ma, "Preparation and mechanism study of ZnO ammonia gas

sensor based on precious metal nanoparticles (AuNPs, AgNPs) modification," *Journal of Alloys and Compounds*, vol. 1010, p. 177613, 2025.

[29] J. Dong, J. Guo, T. Shao, H. Kou, Y. Cheng, F. Zhang, X. Liu, and S. Tian, "Enhanced ethanol gas sensing performance of Ag/SnO_2 composites," *Sensors and Actuators B: Chemical*, vol. 423, p. 136721, 2025.

[30] Y. Liu, X. Li, X. Li, C. Shao, C. Han, J. Xin, D. Lu, L. Niu, Y. Tang, and Y. Liu, "Highly permeable WO_3/$CuWO_4$ heterostructure with 3D hierarchical porous structure for high-sensitive room-temperature visible-light driven gas sensor," *Sensors and Actuators B: Chemical*, vol. 365, p. 131926, 2022.

[31] Y. Tang, Z. Han, Y. Qi, Z. Yang, H. Han, Y. Jiang, X. Zhang, L. Wu, Z. Wang, J. Liu, and F. Wang, "Enhanced ppb-level formaldehyde sensing performance over Pt deposited SnO_2 nanospheres," *Journal of Alloys and Compounds*, vol. 899, p. 163230, 2022.

[32] W. Liu, X. Si, Z. Chen, L. Xu, J. Guo, L. Wei, G. Cheng, and Z. Du, "Fabrication of a humidity-resistant formaldehyde gas sensor through layering a molecular sieve on 3D ordered macroporous SnO_2 decorated with Au nanoparticles," *Journal of Alloys and Compounds*, vol. 919, p. 165788, 2022.

[33] C. Liu, Q. Kuang, Z. Xie, and L. Zheng, "The effect of noble metal (Au, Pd and Pt) nanoparticles on the gas sensing performance of SnO_2-based sensors: a case study on the {221} high-index faceted SnO_2 octahedra," *CrystEngComm*, vol. 17, no. 33, pp. 6308-6313, 2015.

[34] S. Limwichean, P. Eiamchai, C. Ponchio, N. Kasayapanand, and M. Horprathum, "Comparative investigations of DCMS/HiPIMS reactively sputtered WO_3 thin films for photo-electro-chemical efficiency enhancements," *Vacuum*, vol. 185, p. 109978, 2021.

[35] T. Hyodo, T. Goto, M. Takamori, T. Ueda, and Y. Shimizu, "Effects of Pt loading onto SnO_2 electrodes on CO-sensing properties and mechanism of potentiometric gas sensors utilizing an anion-conducting polymer electrolyte," *Sensors and Actuators B: Chemical*, vol. 300, 2019.

[36] Ö. Şahin, A. Akdağ, S. Horoz, and A. Ekinci, "Physical and electrochemical effect of bimetallic Pd–Mo nanoalloys supported on Vulcan XC-72R carbon as cathode catalysts for proton exchange membrane fuel cell," *Electrocatalysis*, vol. 14, no. 2, pp. 202-212, 2023.

[37] H. Ren, S. Tao, H. Pan, J. Huang, and S. W. Joo, "Template preparation of porous Pt-modified SnO_2 microflowers for high-response detection of VOCs," *Materials Research Bulletin*, vol. 170, 2024.

[38] R. Lotfi Orimi, and M. Maghouli, "Optical characterization of SnO_2 nanostructure thin films, annealed at different temperatures," *Optik*, vol. 127, no. 1, pp. 263-266, 2016.

[39] N. Zingwe, E. Meyer, and J. Mbese, "Evaluating the efficacy of binary palladium alloy PdO-Pd for use as an electrocatalyst in DSSC counter electrodes," *South African Journal of Chemical Engineering*, vol. 37, pp. 92-97, 2021.

[40] B. Samransuksamer, T. Jutarosaga, M. Horprathum, A. Wisitsoraat, P. Eiamchai, S. Limwichean, V. Patthanasettakul, C. Chananonnawathorn, and P. Chindaudom "Highly sensitive H_2 sensors based on Pd- and PdO-decorated TiO_2 thin films at low-temperature operation," *Key Engineering Materials*, vol. 675-676, pp. 277-280, 2016.

[41] H. H. Kan, and J. F. Weaver, "Mechanism of PdO thin film formation during the oxidation of Pd (111)," *Surface Science*, vol. 603, no. 17, pp. 2671-2682, 2009.

[42] C. Ke, W. Zhu, J. S. Pan, and Z. Yang, "Annealing temperature dependent oxygen vacancy behavior in SnO_2 thin films fabricated by pulsed laser deposition," *Current Applied Physics*, vol. 11, no. 3, pp. S306-S309, 2011.

[43] Q. Wang, C. Wang, H. Sun, P. Sun, Y. Wang, J. Lin, and G. Lu, "Microwave assisted synthesis of hierarchical Pd/SnO_2 nanostructures for CO gas sensor," *Sensors and Actuators B: Chemical*, vol. 222, pp. 257-263, 2016.

[44] Q. Wang, L. Bao, Z. Cao, C. Li, X. Li, F. Liu, P. Sun, and G. Lu, "Microwave-assisted hydrothermal synthesis of Pt/SnO_2 gas sensor for CO detection," *Chinese Chemical Letters*, vol. 31, no. 8, pp. 2029-2032, 2020.

[45] S. Peng, P. Hong, Y. Li, X. Xing, Y. Yang, Z. Wang, T. Zou, and Y. Wang, "Pt decorated SnO_2 nanoparticles for high response CO gas sensor under the low operating temperature," *Journal of Materials Science: Materials in Electronics*, vol. 30, no. 4, pp. 3921-3932, 2019.

[46] A. Gurlo, "Interplay between O_2 and SnO_2: Oxygen ionosorption and spectroscopic evidence for adsorbed oxygen," *ChemPhysChem*, vol. 7, no. 10, pp. 2041-2052, 2006.

[47] A. K. Gangwar, R. Godiwal, S. Srivastava, P. Pal, G. Gupta, and P. Singh, "Preparation of nanocrystalline Pd/SnO_2 thin films deposited on alumina substrate by reactive magnetron sputtering for efficient CO gas sensing," *Materials Research Bulletin*, vol. 148, p. 111692, 2022.

[48] M. H. Saberi, Y. Mortazavi, and A. A. Khodadadi, "Dual selective Pt/SnO_2 sensor to CO and propane in exhaust gases of gasoline engines using Pt/$LaFeO_3$ filter," *Sensors and Actuators B: Chemical*, vol. 206, pp. 617-623, 2015.

[49] K. C. Lee, Y. J. Chiang, Y. C. Lin, and F. M. Pan, "Effects of PdO decoration on the sensing behavior of SnO_2 toward carbon monoxide," *Sensors and Actuators B: Chemical*, vol. 226, pp. 457-464, 2016.

[50] S. Ghosh, M. Narjinary, A. Sen, R. Bandyopadhyay, and S. Roy, "Fast detection of low concentration carbon monoxide using calcium-loaded tin oxide sensors," *Sensors and Actuators B: Chemical*, vol. 203, pp. 490-496, 2014.

[51] D. T. Do, N. D. Hoa, P. V. Tong, N. V. Duy, T. D. Dao, H. V. Chung, T. Nagao, and N. V. Hieu, "Effective decoration of Pd nanoparticles on the surface of SnO_2 nanowires for enhancement of CO gas-sensing performance," *Journal of Hazardous Materials*, vol. 265, pp. 124-132, 2014.

[52] Y. C. Lee, H. Huang, O. K. Tan, and M. S. Tse, "Semiconductor gas sensor based on Pd-doped SnO_2 nanorod thin films," *Sensors and Actuators B: Chemical*, vol. 132, pp. 239-242, 2008.

[53] C. Liewhiran, N. Tamaekong, A. Wisitsoraat, A. Tuantranont, and S. Phanichphant, "Ultra-sensitive H_2 sensors based on flame-spray-made Pd-loaded SnO_2 sensing films," *Sensors and Actuators B: Chemical*, vol. 176, pp. 893-905, 2013.

[54] Z. Wang, Z. Li, T. Jiang, X. Xu, and C. Wang, "Ultrasensitive hydrogen sensor based on Pd(0)-loaded SnO_2 electrospun nanofibers at room temperature," *ACS Applied Materials & Interfaces*, vol. 5, no. 6, pp. 2013-2021, 2013.

[55] S. Das, D. Sarkar, and D. Basak, "Pt nanoparticles decorated SnO_2 nanoneedles for efficient CO gas sensing applications," *Sensors and Actuators B: Chemical*, vol. 256, pp. 656-664, 2018.